Tailoring the dielectric and ferroelectric response of mixtures containing bent-core liquid crystals through light-irradiation and composition.

Jasmin Liebsch [a,b], Rebecca Strachan [a], Sivanujan Suthaharan [c], Ivan Dominguez-Candela [d, e], Carlota Auria-Soro [f], Andres San-Millan [a], Rebecca Walker [b], Bhaskar Chilukuri [c], M. Blanca Ros [f], Alfonso Martinez-Felipe [a,g]*

[a] *School of Engineering, King's College, University of Aberdeen, Aberdeen, AB24 3UE, Scotland, UK.*

[b] *Department of Chemistry, School of Natural and Computing Science, Meston Walk University of Aberdeen, Aberdeen, AB24 3UE, Scotland, UK.*

[c] *Department of Chemistry, Illinois State University, Normal, IL 61790-4160, USA.*

[d] *Instituto de Seguridad Industrial, Radiofísica y Medioambiental (ISIRYM) Universitat Politècnica de València (UPV), Plaza Ferrándiz y Carbonell, s/n 03801 Alcoy, Spain.*

[e] *Technological Institute of Materials (ITM), Universitat Politècnica de València (UPV), Plaza Ferrándiz y Carbonell 1, 03801 Alcoy, Spain.*

[f] *Instituto de Nanociencia y Materiales de Aragón, Departamento de Química Orgánica, Facultad de Ciencias, Universidad de Zaragoza-CSIC, Campus San Francisco, E-50009 Zaragoza, Spain.*

[g] *Chemical Materials and Processes Group, Just Transition Lab, University of Aberdeen, Aberdeen, AB24 3UE, Scotland, UK.*

** corresponding author: a.martinez-felipe@abdn.ac.uk*

ABSTRACT

We report the mesomorphic behaviour, dielectric and ferroelectric properties, and computational modelling of binary mixtures containing two bent-core liquid crystals: the so-called NG75-COO (3,4´- Bis[4-(4-n-tetradecyloxybenzoyloxy)benzoyloxy]biphenyl), which forms smectic phases, and IP31- AzB (3,4' - Bis[4-(4-n-tetradecyloxyphenylazo)benzoyloxy]biphenyl), which forms columnar phases. The phase diagram, assessed by polarised optical microscopy, shows that the binary mixtures retain the mesophase behaviour of the major component, whilst the equimolar mixture displays smectic-type phases. Dielectric and ferroelectric analyses were carried out on samples containing 10%, 50%, and 90% of IP31-AzB (molar %), and we also investigated structure-property correlations by differential functional theory. The NG75-COO/IP31-AzB mixtures undergo strong dielectric and ferroelectric response due to the presence of highly polarisable groups in the bent-core components, particularly at the ester groups. All the mixtures under study exhibit light-responsiveness induced by reversible *E*-to-*Z* photoisomerization (*trans*-to-*cis*) of the azobenzene group in IP31-AzB, together with an increase in the molecular dipole moment. The potential to tune the phase behaviour of the mixtures, as well as their dielectric and ferroelectric responses, are investigated by light irradiation under different conditions of intensity and temperature.

Keywords: azobenzenes, bent-core liquid crystals, ferroelectricity, dielectric spectroscopy, energy storage, density functional theory.

1. Introduction

Liquid crystals are excellent candidates as soft materials for energy devices, due to their capability to form multiscale nanostructures that respond to external stimuli, with the potential to switch between several functionalities.[1] Liquid crystals can display very attractive technological properties, such as, ferroelectricity, flexoelectricity, piezoelectricity,

ionic and electric conductivity, which can be tuneable through physical variables, such as, temperature, light, or electrical and magnetic fields. [2, 3] Distinctively, they allow to create controlled 1D (columnar) [4], 2D (smectic) [5] and 3D (bicontinuous) [6] channels that, for example, can promote transport of ions or charges in electrolytes, and their application in fuel cells [7-14], solar cells[15-17], batteries [18-21], wearable energy devices [22], among others [23-25].

With this aim, we have recently postulated the potential of bent-core liquid crystals (BCLCs) for their use in energy conversion and storage devices.[26, 27] Even since their discovery back in the 1990's [28-36], BCLCs continue to attract interest from both fundamental and practical grounds. The molecular designs of BCLCs facilitate compact molecular packing and lead to biaxial properties. In addition, the relative orientation of polar groups present at the bent-core structure respect to its molecular axes promotes the appearance of local dipole moments leading to distinctive polar organisations. BCLCs can form a variety of mesophases, including columnar (Col, former B1), polar smectic C (SmCP, former B2), twist grain boundary dark conglomerate (DC) or helical nanofilament (HNF, former B4) [29-32, 35-37], whose appearance depends strongly on molecular design. Furthermore, despite their non-chiral molecular nature, some BLCSs tend to exhibit ferroelectric response upon the application of external electrical fields, assisted by the formation of compact packing arrangements that restrict rotational freedom. [28, 34, 35, 37]

As part of our systematic research to explore new structure – properties relationships, in a recent work, we studied new BCLC materials based on mixtures of a classic bent-core mesogen, the so-called NG75-COO compound. [26] Physical mixing offers a versatile pathway to create and test new functional materials, avoiding some costly synthetic steps. Intriguingly, whilst there are plenty of studies in the literature about mixing bent-core and calamitic liquid crystals, examples of mixtures of bent-core components are more limited. [38-41] Thus, we prepared mixtures of NG75-COO, which forms a SmCP mesophase, containing 5% molar composition of two other BCLCs bearing azobenzene groups, the so-called IP31-AzB (forming a columnar phase) and IP33-AzB (forming a smectic C polar

phase), in order to yield new light-responsive materials.[42-44] Our results confirmed the potential of these 5% azo-containing mixtures to combine ferroelectric and light-response, which could be used to promote phase transitions upon illumination and modulation of their properties.

In this work, we focus on one of these mixtures, namely the NG75-COO/IP31-AzB system, and we carry out a full compositional analysis. Therefore, our aim is two-fold. On the one hand, we will perform a fundamental investigation of the compatibility of the two pristine compounds and the phase behaviour of the mixtures. On the other hand, we will study the effect of composition on the dielectric and ferroelectric response of selected mixtures, with particular focus on their light-response, as a strategy to assess their potential performance as light-harvesting components for energy applications.

2. Experimental section

Materials

The two pristine bent-core compounds used in this work are structurally close, containing six aromatic rings and ester bonds to build the rigid-bent core, and two long flexible chains (-OC14H29). Both compounds were previously reported [45-49] and designated as: NG75-COO (3,4´- Bis[4-(4-n-tetradecyloxybenzoyloxy)benzoyloxy]biphenyl, non-photosensitive) and IP31-AzB (3,4' - Bis[4-(4-n-tetradecyloxyphenylazo)benzoyloxy]biphenyl, containing two photo-responsive azobenzene groups), see **Fig. 1.** Their synthesis is summarised as Electronic Supplementary Information (**Scheme S1**). NG75-COO forms a smectic C polar phase (SmCP), while IP31-AzB develops an obliquus columnar phase (Colob), and the transition temperatures reported from the literature are also summarised in **Fig. 1**. Up to nine binary mixtures were prepared for the current study by weighting the corresponding solid components, mixing them in a common solvent, and allowing for evaporation of the solvent under stirring. Samples were then further dried in a vacuum oven for 24 hours.

These mixtures are labelled as *X*%-IP31-AzB, where *X* is the molar percentage of the azobenzene component IP31-AzB. 0%-IP31-AzB corresponds to pristine NG75-COO, and 100%-IP31-AzB corresponds to pristine IP31-AzB.

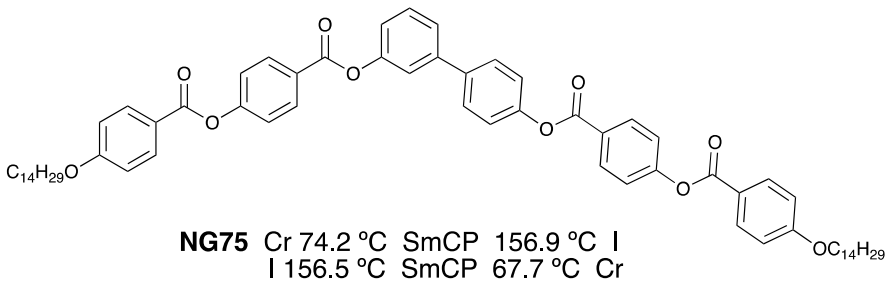

NG75 Cr 74.2 ºC SmCP 156.9 ºC I
I 156.5 ºC SmCP 67.7 ºC Cr

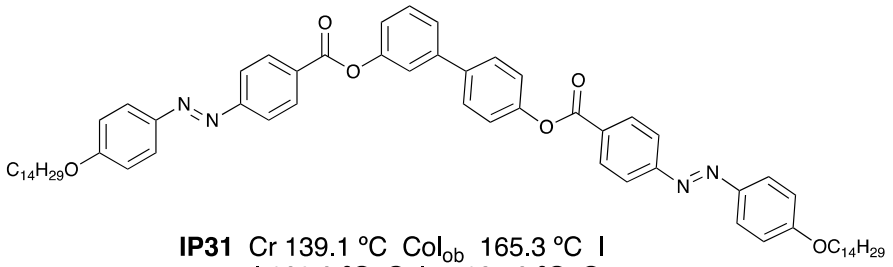

IP31 Cr 139.1 ºC Col_{ob} 165.3 ºC I
I 160.9 ºC Col_{ob} 127.8 ºC Cr

Figure 1. Chemical structures of the pristine bent-core liquid crystals used in this work and their phase transition data reported in the literature: NG75-COO [47, 48] and IP31-AZB [45] (Cr: crystal; Colob: obliquus columnar; SmCP: smectic C polar; I: isotropic)

Methods and instruments

The phase behaviour of the mixtures was determined by polarised optical microscopy (POM), using an Olympus Bx5m microscope with a cross polariser. Microscopic, dielectric, and ferroelectric tests were carried out for Indium Tin Oxide (ITO) cells (Instec S025A032uG180) containing the *X*%-IP31 samples (see **Figure S1**). The cells were filled by capillary action from the melt and connected to the instruments by two aluminium foil electrodes attached using RS PRO silver conductive paint. Cells have an active area of $\mathrm{A} = 25\ \mathrm{mm}^2$, thickness of $\mathrm{h} = 3.2\ \mu\mathrm{m}$, resistance of 100Ω, and their overall capacitance, C_O can be calculated as:

$$C_O = \frac{\varepsilon_O A}{h} = 1.11 \times 10^{-10}\mathrm{F} \qquad \text{Eq. 1}$$

with $\varepsilon_o = 8.854 \times 10^{-12} F \cdot m^{-1}$ is the permittivity of vacuum. Temperature was controlled by placing the ITO cells on top of a Linkam THMS 600 heating stage combined with a TMS 91 control unit, with ±0.1ºC accuracy.

The dielectric response was obtained by complex impedance spectroscopy, using a Solartron Modulab XM frequency response analyser (FRA). Frequency sweeps ranged from 0.01 to 10^6 Hz, using alternating fields of 1 Vrms amplitude; some additional isothermal experiments were taken at a fixed frequency of 5 kHz, in the time domain. The ferroelectric response was acquired through a Radian RT66C Test System ferroelectric analyser. The polarisation of the cells was measured through hysteresis loops of sinusoidal fields in the ±75 kV·cm^{-1} range, and at different frequencies. The UV light was irradiated to the samples using a Dymax Bluewave QX4 TM LED pot-curing system, which can be set up with a Dymax ACCU-CALTM 50-LED instrument. The UV-visible spectra were obtained on a Cary 50 Scan UV-vis spectrophotometer (Agilent Technologies). Further details on the experiments can be found in the results section.

To understand the role of electronic structure in the aggregation and phase behaviour of our samples, we performed molecular density functional theory (DFT) calculations on modified (*vide infra*) molecular models of the BCLC components in **Fig. 1**. Gas-phase DFT calculations were performed using Gaussian09 [50], with empirical dispersion-corrected B97D [51] generalised gradient approximation (GGA) functional. B97D is established as a hybrid GGA functional which is dispersion-corrected *via* explicit parametrisation. Several studies [52-54] indicate that B97D yields accurate description of molecular properties and exhibits a good performance in reproducing structural geometries. These investigations also show that B97D eliminates systematic overestimation of internuclear distances, which is a common problem often seen in dispersion-excluded standard DFT calculations. All atoms

were modelled using 6-31G(d) Pople basis set. [55] Geometry optimisations of ground state molecular models were performed and no imaginary frequencies were observed for the optimised structures, as confirmed by calculation of the energy Hessian. Additionally, single-point calculations of the corresponding ionic and excited state structures were performed to assess the electronic structure and polarisability of the BCLCs, as detailed in the supplementary information.

3. Results and discussion

3.1. Phase behaviour

Initially, a contact preparation study of the two bent-core components was carried out under the polarizing microscope in a cooling process from a temperature where both pure components and mixtures were in the isotropic liquid phase. As the sample was cooled, first the zone corresponding to IP31 showed the formation of a texture identified as a Col mesophase while at lower temperature, the zone corresponding to NG75 offered the formation of defects which agree with a SmCP organization. Both birefringent areas were separated by a black isotropic one that disappears becoming birefringent on cooling at lower temperatures, **Fig. 2**. Interestingly, neither black zones nor new textures were observed above 150 ºC suggesting the good mixing of both components in the whole range of blending, but the persistence of just Col or SmCP mesophases.

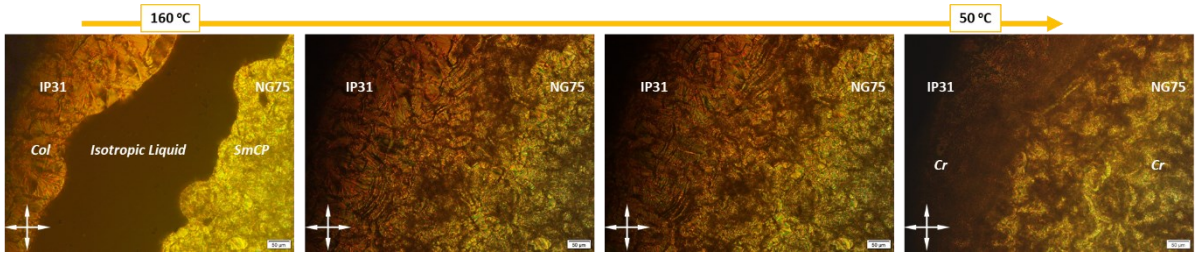

Figure 2. Optical textures between crossed polarizers of a contact preparation of IP31-AzB and NG75-COO between two glass plates, uncoated cells, in a cooling process at 10º·min-1 from isotropic liquid phases. Red scale equals 50 µm.

In order to quantify their phase behaviour, up to nine binary mixtures (10, 20, 30, 40, 50, 60, 70, 80 and 90 % molar of NG75) were prepared and studied under the polarized microscope, in either ITO or glass cells, while cooling at -1 C·min^{-1}. All NG75/IP31 mixtures show birefringence under the microscope, with textures that flash under pressure between glasses, which confirms the formation of liquid crystalline mesophases. At sufficiently low temperatures, all samples crystallise. Samples with high NG75 concentrations develop textures, **Fig. 3(a)**, some of which could be consistent with the formation of SmCP phases, whilst samples with high concentrations of IP31 exhibit recognizable banana-leaf textures, **Fig. 3(c)**, consistent with columnar mesophases, which we have labelled as Col. Mixtures with intermediate compositions show less well-defined textures, **Fig. 3(b)**, but consistent with a SmCP phase assignation based on their formation process. Mixtures with high IP31 contents (>50% molar), on the other hand, show transitions, which can be correlated to isotropic to columnar, and columnar to crystal transitions.

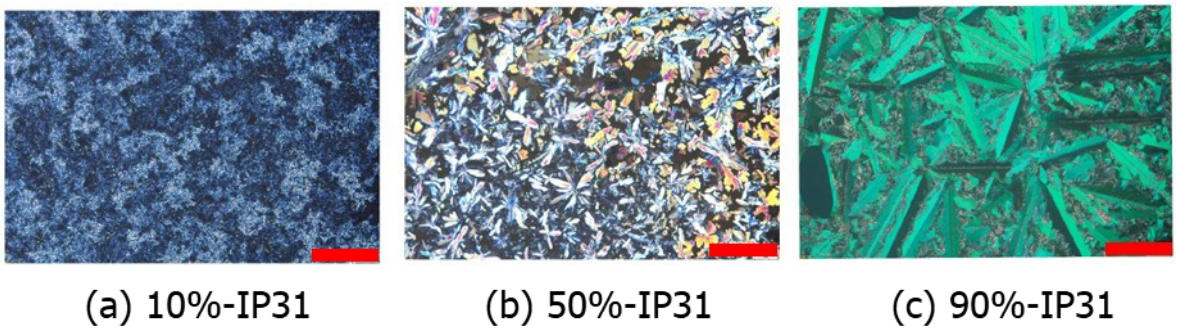

Figure 3. Optical textures between crossed polarizers of selected mixtures in ITO cells: (a) 10%-IP31 (120 ºC) ; (b) 50%-IP31 (80 ºC); and (c) 90%-IP31 (160 ºC). between ITO coated cells. Red scale represents 500 μm.

A phase diagram was prepared, based on POM observations made on cooling, and is shown in **Fig. 4**. The presence of the second component destabilises in all cases the mesophase ($\Delta T_{I\text{-}Mesophase}$~ -20ºC), but in these samples the liquid crystalline range remains broad (~ 25ºC). These effects will be studied in a further section of the manuscript when we carry out

a DFT analysis. Taking into account this phase behaviour, we will use three representative samples to study the effect of composition on the photoelectrical response of the NG75/IP31 series: 10%-IP31, to assess the introduction of low concentrations of azobenzene units on a smectic-type mixture; 90%-IP31, to analyse the effect of small amounts of NG75 on a columnar-type mixture; and 50%-IP31, to study the equimolar composition.

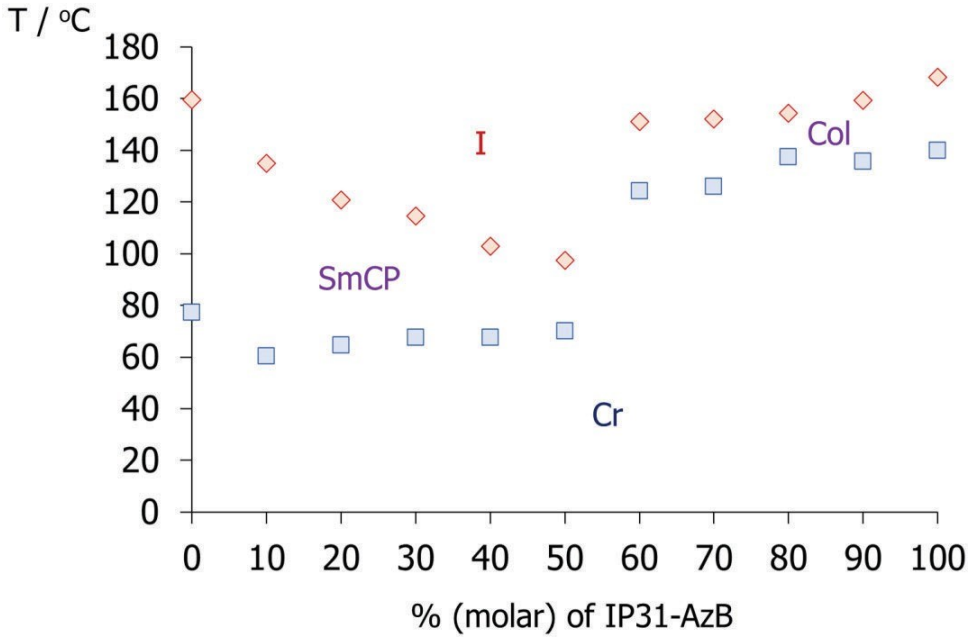

Figure 4. Phase diagram corresponding to the NG75/IP31 mixtures, obtained on cooling from the isotropic melt, based on polarised microscopy observations (-1ºC·min^{-1}): Isotropic (I); Smectic C Polar (SmCP); Columnar (Col); Crystal (Cr).

3.2. Dielectric and ferroelectric response

The dielectric response of the mixtures was assessed using the complex dielectric permittivity:

$$\varepsilon^* = \varepsilon' - i\,\varepsilon''$$

where ε' is the dielectric elastic constant, ε'' is the loss factor, and *i* is the complex unit. The complex conductivity was also calculated according to:

$$\sigma^* = \sigma' + i\,\sigma''$$

considering that:

$$\sigma' = i\,\omega\varepsilon''$$

with ω is the radial frequency of the alternating electrical field, in rad·s^{-1}. Direct conductivity (DC) values, σ_{dc}, were estimated from the plateaus at doble logarithmic σ' *vs* frequency plots.

Fig. 5 shows two-dimension (2D) and three-dimension (3D) plots corresponding to the dielectric loss factor, ε'' (relative to ε_0), of the selected mixtures obtained on isothermal frequency sweeps on cooling from their isotropic melts. The isothermal plots for the dielectric elastic constant, ε' (relative to ε_0), and the real component of the complex conductivity, σ', can be found as supplementary information (**Fig. S2** and **S3**, respectively). The values of the loss factor, ε'', fall within the range of other bent-core liquid crystalline materials [56, 57]. Their dielectric response can be attributed to the reorientation of permanent dielectric dipoles perpendicular to the long molecular axes, and also internal rotations in the NG75 and IP31 molecules [58, 59]. More specifically, NG75 shows direct conductivity (DC) values up to $\sigma_{dc} \sim 10^{-5}$ S cm^{-1} (at low frequencies) and above 10^{-3} S·cm^{-1} (at high frequencies), see **Fig. S3**.[53] The increase in conductivity at higher temperatures must be due to thermal activation of localized charge carriers, which contribute to dielectric polarization. [60] Our σ_{dc} values fall within the high range found for liquid crystalline materials, and even comparable to ionic liquid crystals and salts reported in our own lab, [12-14, 61-63] and we will return to this observation later.

As expected, the mixtures display several dielectric processes that can be identified, to some extent, with those of the pristine components.[26] 10%-IP31-AzB, **Fig. 5(a)**, has composition and dielectric response that resemble those of NG75-COO, with two dielectric processes that appear in comparable temperature/frequency ranges to the pristine compound, as reported by us in [26]. More specifically, we have assigned those processes to α and β relaxations (in decreasing temperature order). The α-relaxation is associated to

a Goldstone(phason)-mode relaxation involving cooperative motions of the molecules within the smectic layers, without varying the tilt angle. [56, 57, 64, 65] The β process typically manifests in a narrow temperature range and at higher frequencies can be associated to a soft(amplitude)-mode relaxation, when molecules vary their tilt angle within the same plane. 50%-IP31 shows a very well-defined ε'' response, with a main relaxation in the mid-frequency relaxation that exhibits Vogel-Fulcher-Tamman (VFT) behaviour in the Arrhenius plots of **Fig. 6**, indicating that the molecular motions are controlled by viscous forces.[60, 61] For this mixture, we have calculated an activation energy of E_a = 41.2 kJ mol^{-1} in the linear region, according to:

$$\ln(f_{max}/Hz) = A - \frac{E_a}{R} \cdot \frac{1}{T}$$

where f_{max} is the maximum frequency at each ε'' curve, T is the temperature in Kelvin, R is the gas constant, and A is a pre-exponential term.

This value is again comparable with that reported for NG75-COO (47.9 kJ mol^{-1}), which is consistent with an α-relaxation. The value obtained for the crystal phase is much higher (101.3 kJ mol^{-1}), denoting an increase in intermolecular forces and constrain in molecular mobility. Unfortunately, we could not measure the activation energy of the β process for our 10%-IP31-AzB sample.

90%-IP31-AzB has comparable composition and dielectric response to pristine IP31-AzB, see **Fig. 5(c)**. One main dielectric process can be seen, which we have assigned to the β relaxation reported for pristine IP31-AzB in [26], based on the temperature/frequency window when it appears. The activation energy calculated for 90%-IP31-AzB (87.3 kJ mol^{-1}) is much lower than that reported for IP31-AzB (161.0 kJ mol^{-1}). We believe that this difference may be caused by a certain destabilisation of the columnar order due to the presence of NG75-COO molecules in the mixture, which is consistent with the depression in the clearing and crystallisation temperatures depicted in **Fig. 4**.

50%-IP31-AZB, on the other hand, shows a very well-defined ε'' process in **Fig. 5(b)**, which can be explained in terms of its equimolar composition. At high temperatures, in its isotropic melt, this process has little or no temperature dependence. On cooling below the sample's clearing point ($T_{I\text{-}SmC}$ = 110°C), a relaxation peak shifts to lower frequencies, with an apparent activation energy of 48.3 kJ mol^{-1}. This E_a value (in the ~50 kJ mol^{-1} range), as well as the temperature/frequency window when the process appears, are in excellent agreement with those of the α relaxation reported for pristine NG75-COO and our 10%-IP31- AzB sample, and with those reported for other smectic materials.[57]. The permittivity undergoes another step-change at around 80°C, which can be associated to crystallisation of the sample, T_{cr}, with an activation energy of further cooling consistent to that calculated for pristine NG75-COO (86.5 kJ mol^{-1}) [26].

Hence, it is very likely that the molecular origin of the dielectric response of 50%-IP31-AzB is similar to that of NG75-COO, which is consistent with our hypothesis that mixtures with 50% and higher NG75-COO molar concentrations form smectic-type nanostructures. The absence of a clear β relaxation in the equimolar sample can be explained by the heterogeneous local environment of the bent-core molecules, which may restrict tilt-angle variations, but also by the shift in the temperature of the relaxation in the mixture, which may push this process out of the current temperature/frequency experimental window. The presence of the ε'' peak above the clearing point observed by POM ($T_{I\text{-}SmC}$=110°C) is somehow intriguing, and may reflect pre-transitional effects that are not observable under the microscope, including the nucleation of short-range smectic arrays on cooling below the clearing point of the individual components.

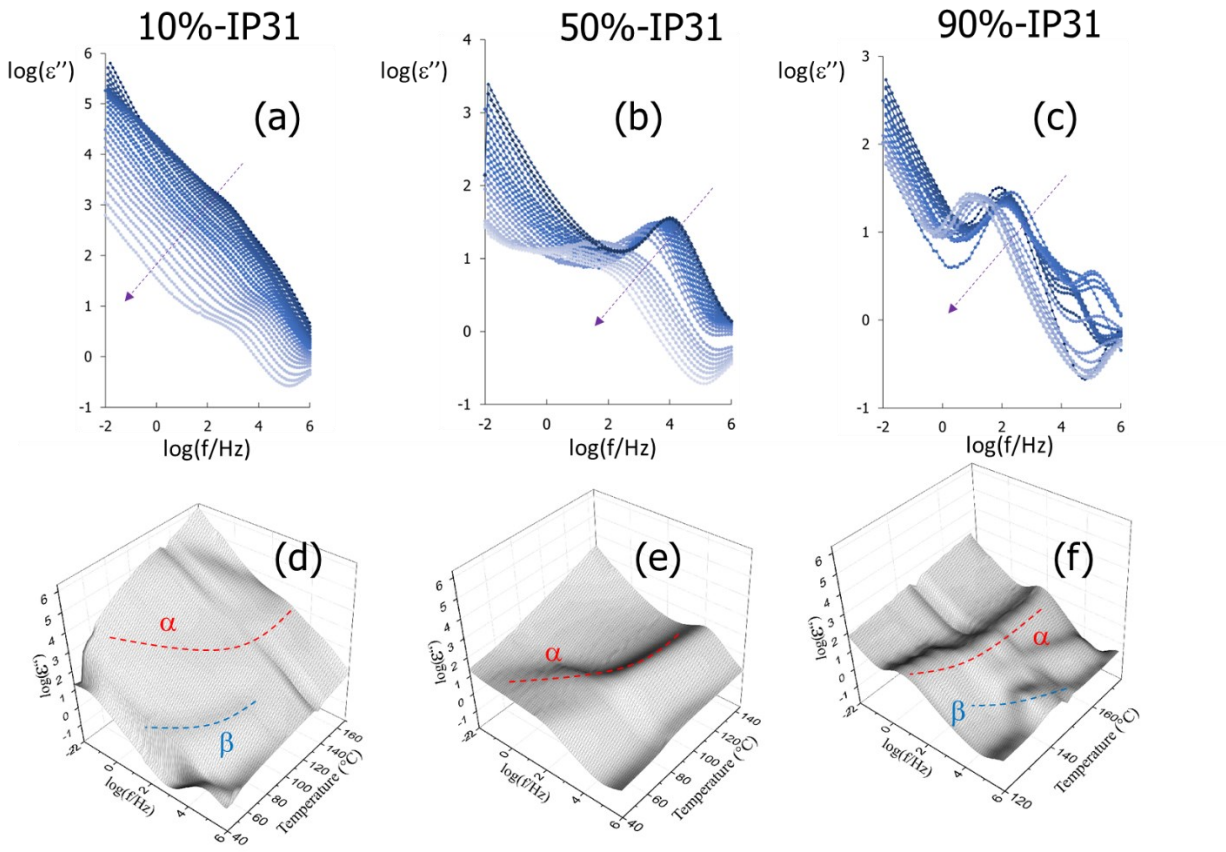

Figure 5. 2D-plots (**a** to **c**) and 3D-plots (**d** to **f**) showing the dielectric loss factor, ε'', as a function of frequency and temperature, corresponding to 10%-IP31 (a, d); 50%-IP31 (b, e); 90%-IP31 (c, f); obtained in isothermal steps, on cooling from their isotropic phases (arrows indicate direction on cooling). Dielectric α and β relaxations are highlighted.

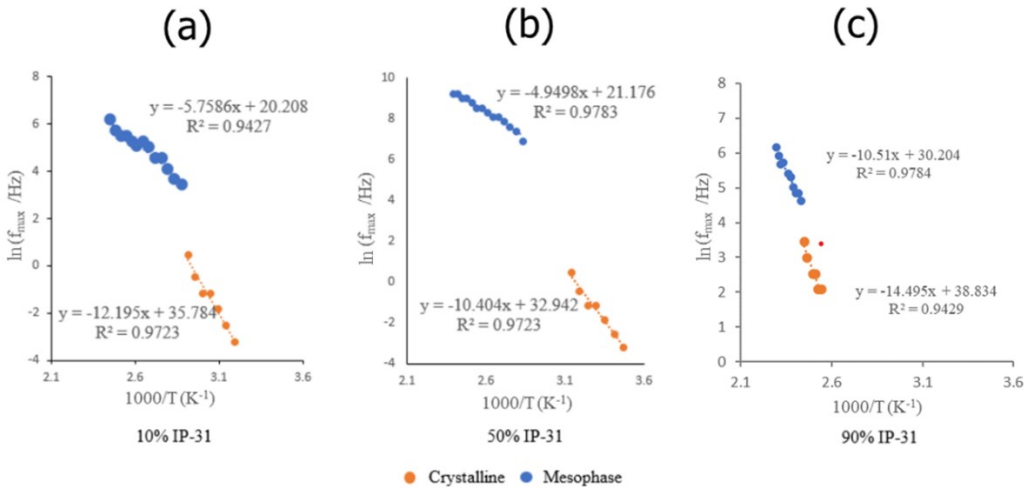

Figure 6. Arrhenius plots obtained for the maxima (f_{max}) of the dielectric loss factor curves, ε'', of the mixtures under study.

We also note that 10%-IP31 displays stronger dielectric and conductivity responses, together with stronger polarizability (see **Table 1**) respect to the other two samples (50%-IP31 and 90%-IP31), illustrated in their respective polarisation loops in **Fig. 7**. Indeed, all mixtures exhibit non-linear polarisation response and remanent polarisation (at zero voltage, P_R) typical of ferroelectric behaviour. The values of P_R and saturated polarisation (P_S, at the highest voltage) are summarised in **Table 1**, where we also show the energy storage capacity (E_S, $J \cdot cm^{-3}$), calculated from the integrated area in the polarization-electric field (P-E) hysteresis loops (see shadowed area in **Fig. 7**). These results are consistent with our previous findings, [26] and confirm that, whilst the ferroelectric (and dielectric) behaviour is weakened at high concentrations of IP31 molecules in the mixtures, they can still retain relaxor response and capacity to store energy, with a maximum obtained for 50%-IP31. These results are also in agreement with our phase model where IP31 molecules are compatible with the SmCP phase developed by NG75, and some amount of IP31 may help stabilise the remanent polarity, possibly by disrupting cooperative motions.

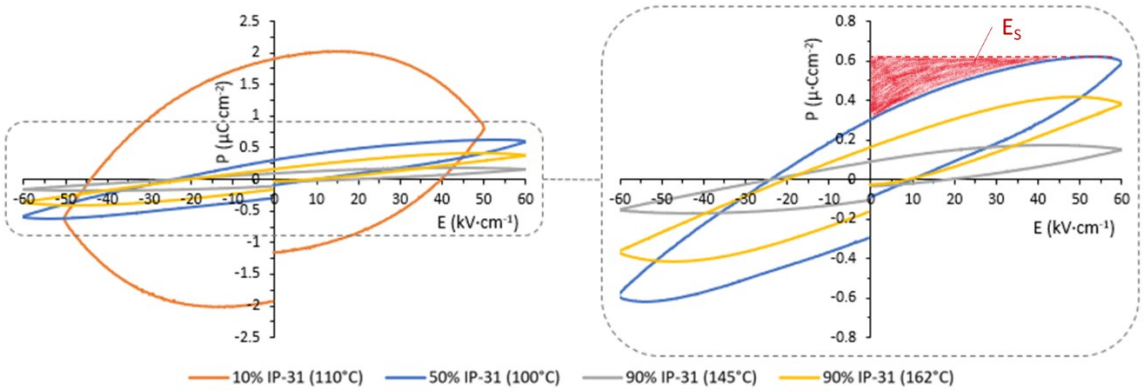

Figure 7. Hysteresis loops and associated showing the ferroelectric response of 10%-IP31 (T=110ºC), 50%-IP31 (T=100ºC), 90%-IP31 (T=145ºC), and 90%-IP31 (T=162ºC), at 20Hz. Shadowed area represents the energy storage capacity (E_S, J·cm^{-3})

Table 1. Ferroelectric parameters obtained from the triangular polarisation loops (75 kV·cm^{-1}; 20 Hz; mesophase range): saturation polarisation (P_S), remanent polarization (P_R) and energy stored (E_S), Energy loss (E_L), for each sample before (a) and during (b) UV irradiation.

(a) No UV irradiation	Saturation polarisation P_S / μC·cm^{-2}	Remanent polarisation P_S/ μC·cm^{-2}	Energy stored E_S / mJ·cm^{-3}
NG75 (135ºC)[27]	0.182	0.0878	2.547
10%-IP31 (110ºC)	2.389	2.244	1.818
50%-IP31 (100ºC)	0.622	0.305	6.031
90%-IP31 (145ºC)	0.172	0.090	1.047
90%-IP31 (162ºC)	0.415	0.162	4.725
IP31 (135ºC)[27]	0.0149	0.681	1.645

(b) Under UV irradiation (1200 mW·cm^{-2})	Saturation polarisation P_S / μC·cm^{-2}	Remanent polarisation P_R / μC·cm^{-2}	Energy stored E_S / mJ·cm^{-3}
10%-IP31	2.714	2.591	0.600
50%-IP31	1.087	0.787	4.519
90%-IP31 (145ºC)	0.290	0.193	0.193
90%-IP31 (162ºC)	0.626	0.411	3.497
IP31 (135ºC) [26]	-0.180	1.510	1.211

3.3. Light response

The azobenzene group in IP31 induces photoresponsive behaviour in the mixtures, and we now perform a detailed investigation of how their structure and functionality can be tuned *via* light irradiation. [66-72] **Fig. 8** displays the UV-vis absorbance measured in tetrahydrofuran (THF) solutions (~10^{-5} M) of the three mixtures under study, at room temperature. All solutions show the strong band associated to the lowest-energy $\pi^* \leftarrow \pi$ transition in the *trans*-azobenzene isomer (~365 nm), and a much smaller intensity absorption peak in the visible region (~440 nm), assigned to a weak $\pi^* \leftarrow n$ transition in the *cis*-azobenzene.[66] We have irradiated the solutions with UV light at 365 nm and 260 mW·cm^{-2}, and have studied the kinetics of excitation, **Fig. 8(a)** to **8(c)**, and relaxation **Fig. 8(d)** to **8(f)**.

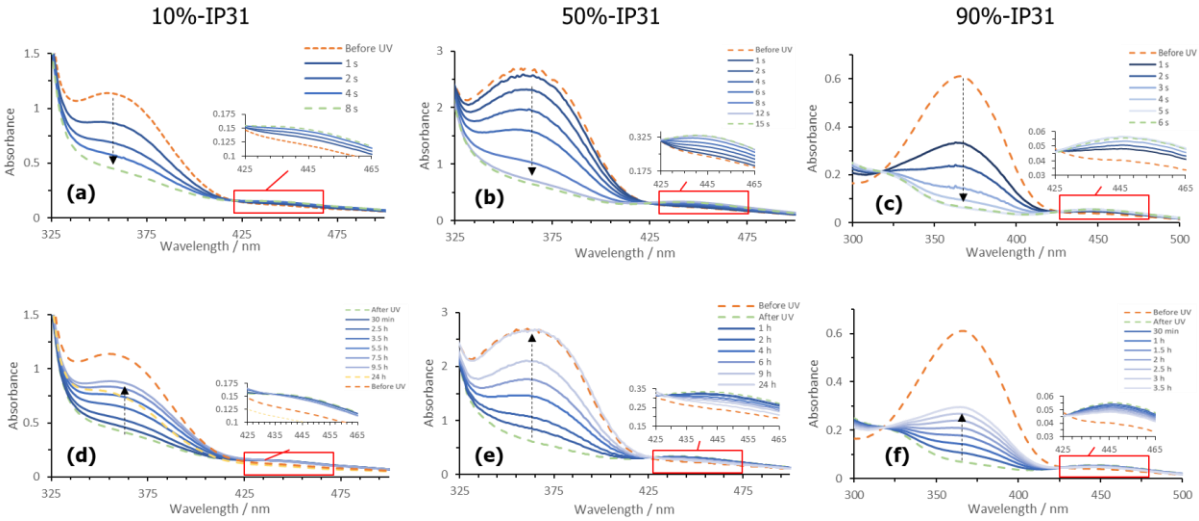

Figure 8. UV-vis spectra of the light-responsive bent-core based mixtures measured in ~10^{-5} M THF solutions at room temperature (10%-IP31: 1.45 x 10^{-4} M; 50%-IP31 and; 90%-IP31: 1.33 x 10^{-4} M). Spectra measured before and at different times after light irradiation (200 mW·cm^{-2}; 365 nm): arrows in **(a)**, **(b)** and **(c)**, shows the excitation during irradiation; arrows in **(d)**, **(e)** and **(f)** indicate signal recovery (relaxation) while samples were kept in the dark.

Upon irradiation, azobenzene undergoes *trans*-to-*cis* photo-isomerisation, evidenced by the rapid decrease in the 365 nm band and the slight increase in the 440 nm region (see inlet in **Fig. 8**). Interestingly, the sample with the highest concentration of azobenzene-component (90%-IP31) displays the slowest excitation process, which may reflect on the lack of cooperativeness of the process. Azobenzene photoisomerisation in solution is a locally activated process, and the longer times required for completion in the 90%-IP31 sample may be due to the higher concentration of groups that need to be excited. Even though *trans*-to-*cis* excitation is fast in all three mixtures (completed in less than one minute), the differences in **Fig 8(a)** to **8(c)** may be relevant in applications when a rapid response is critical, such as, in actuators or sensors.

After irradiation ceases, samples undergo thermally-activated *cis*-to-*trans* back relaxation while kept in the dark, and the UV-vis signals are recovered after 24 h. Relaxation times are longer than excitation (in the hours range) due to the low temperature involved in such a thermally activated process (room temperature). The kinetics of the back relaxation is further assessed by monitoring the maxima of the 365 nm absorbance band, which displays a linear recovery in the logarithmic scale, typical of first order processes, see **Fig. S4**. The half-life values were obtained, $t_{1/2}$, and higher concentrations of IP31 seem to accelerate the *cis*-to-*trans* relaxation, with $t_{1/2}$=6.5 h (10%-IP31), $t_{1/2}$=5.0 h (50%-IP31) and $t_{1/2}$=4.5 h (90%-IP31). Despite the slight differences, the kinetics of all three mixtures fall within the same range.

Fig. 9(a) and **9(b)** illustrates that there are no appreciable textural changes in the POM images for the three current samples upon study when irradiating at moderate intensities (200 $mW \cdot cm^{-2}$). Such stability of *trans*-isomers in these bent-core molecules is consistent with the barriers to promote isothermal phase transitions by light irradiation, which we reported for both IP31 and the 5%-IP31 mixture in [26]. Alternatively, it is possible to promote (at least partial) isotropisation of the 90%-IP31 columnar phase when we irradiate at higher light-intensities (1000 $mW \cdot cm^{-2}$) and at temperatures closer to the clearing point, see the new dark area appearing in **Fig. 9(c)** middle. These results confirm that smectic and

columnar phases appear to be more resilient to UV irradiation that nematic phases, where small dosages promote relevant phase changes. [73, 74]

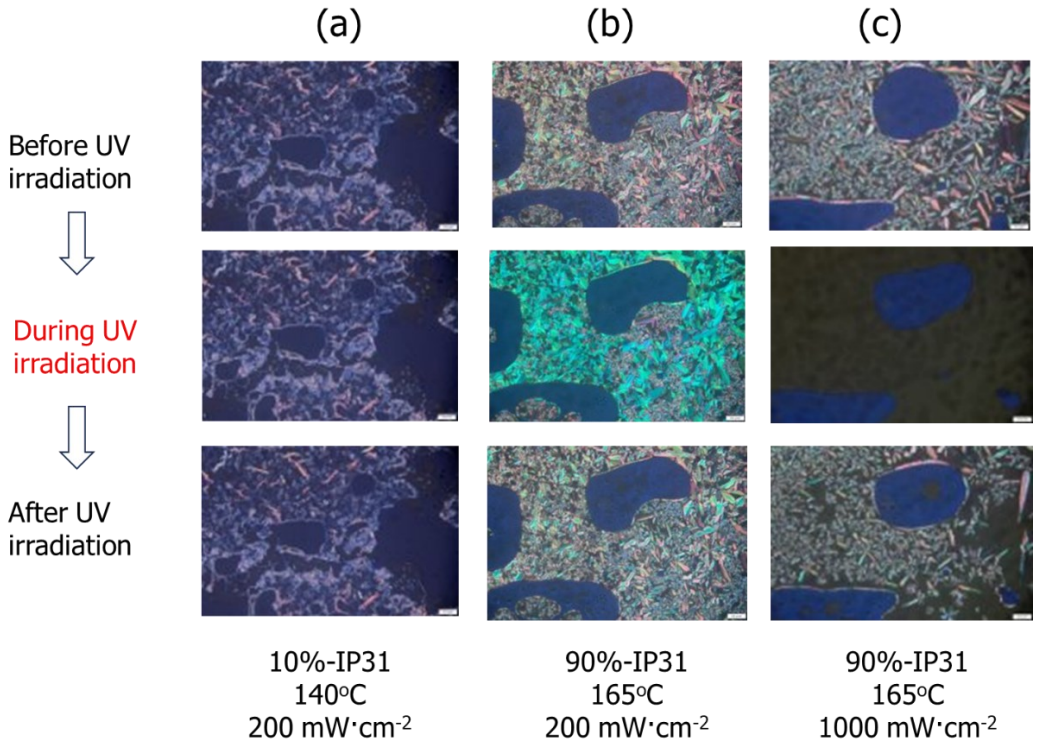

Figure 9. Polarised optical micrographs, POM, of the NG75/IP31 mixtures at different temperatures and under irradiation conditions, showing textural changes (**a** and **b**: 200 mW·cm^{-2}) and partial isotropisation (**c**: 1000 mW·cm^{-2}). Red scale equals to 400 μm.

These results confirm the potential to tune the nanostructure of the mixtures *via* light-irradiation, which could be ultimately used to control their physical properties. The kinetics and reversibility of such changes was further studied in time-dependent experiments, where we monitored the dielectric elastic permittivity (relative to the vacuum value) at a fixed frequency, ε', during irradiation cycles. **Fig. 10(a)** shows how ε' jumps linearly and rapidly upon UV irradiation (UV on, red arrows), reaching a plateau after less than one minute. After switching off light (UV off, blue arrows), ε' decreases following a negative exponential trend, until recovering similar values pre-irradiation. The fast excitation and subsequent slower

relaxation are consistent with the UV-vis spectra discussed in **Fig. 8**, and also with the response displayed by other azobenzene materials. [75, 76] The increase in the dielectric permittivity can be explained by the dipole moment induced in the *cis*-azoisomers, which must contribute to the overall dielectric signal, and this will further discussed in the next section of the manuscript. [77], even though it has also been speculated that continuous *E*-*Z*-*E* photoisomerisations, and the occurrence of iso-mesophase micro transitions, could also improve the dielectric signal. [26] The increase in saturation values at higher intensities in **Fig. 10(a)** reflects on the larger concentration of *cis*-azoisomers, and it is interesting to note that their presence is still compatible with the smectic phases. Comparable responses were obtained for 10%-IP31 and 90%-IP31, see **Fig. S5**, further confirming that the induced *cis*-azoisomers are compatible with the existing liquid crystal order in the mixtures.

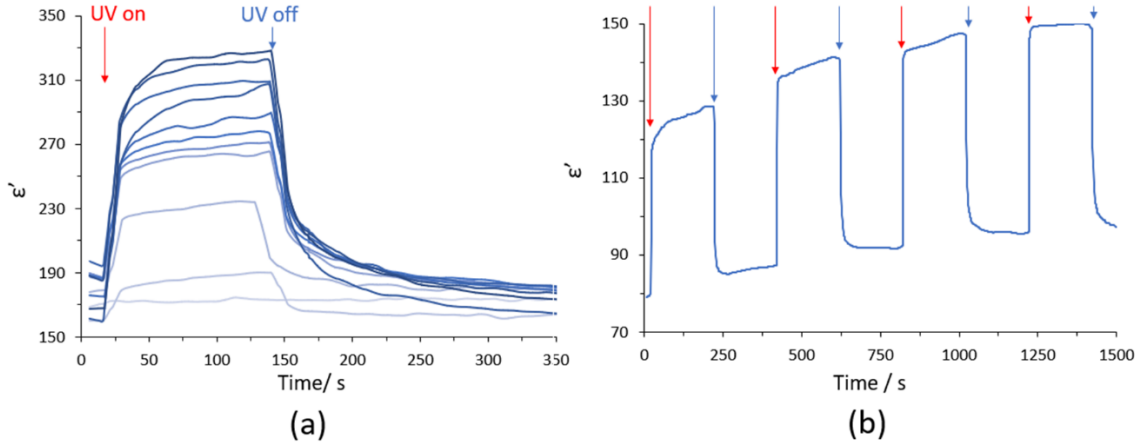

Figure 10. Time-dependence graphs of the dielectric elastic constant, ε' (5 kHz, 100ºC), of 50%-IP31 when submitted to UV off-on-off cycles: **(a)** effect of light intensity, from 200 to 1200 mW·cm^{-2} (dotted arrow); **(b)** cyclic performance during irradiation at 200 mW·cm^{-2}. Baseline shift in (b) may be attributed to a drift caused by the short time interval between experiments.

The increase in ε' reflects that UV light irradiation promotes strong dielectric response in the mixtures, and this also results in higher conductivities, as illustrated for σ' in **Fig. 11**. Even though the conductivity (and dielectric) values are diminished by the introduction of IP31 (respect to NG75, recall **Fig. 5**), it seems that low and moderate concentrations of

azobenzene groups facilitates light-induced conductivity, compare 10%- and 50%-IP31 in **Fig. 11(a)** and **11(b)** More specifically, the reversible performance of 50%-IP31 is consistent with its UV-vis response displayed in **Fig. 10(b)**, and can be useful to design light-responsive electrolytes. Light irradiation also enhances the ferroelectric performance of the mixtures, see **Fig. 12**, with increases in the maximum and remanent polarizations (P_S and P_R, respectively), see **Table 1(b)**. Even though the increase is not dramatic, it is more acute at higher concentrations of IP31, and improve at higher temperatures, **Fig. 12(d)**. It is noteworthy that the potential for energy storage (E_s) is not improved by the effect of light, which aligns with our previous findings for pristine IP31 in [26]. These physical parameters can be tuned to some extent by the intensity of light dosage, as seen in **Fig. 12**. A more detailed study of the combined effect of UV-vis irradiation and temperature will be the object of future investigations.

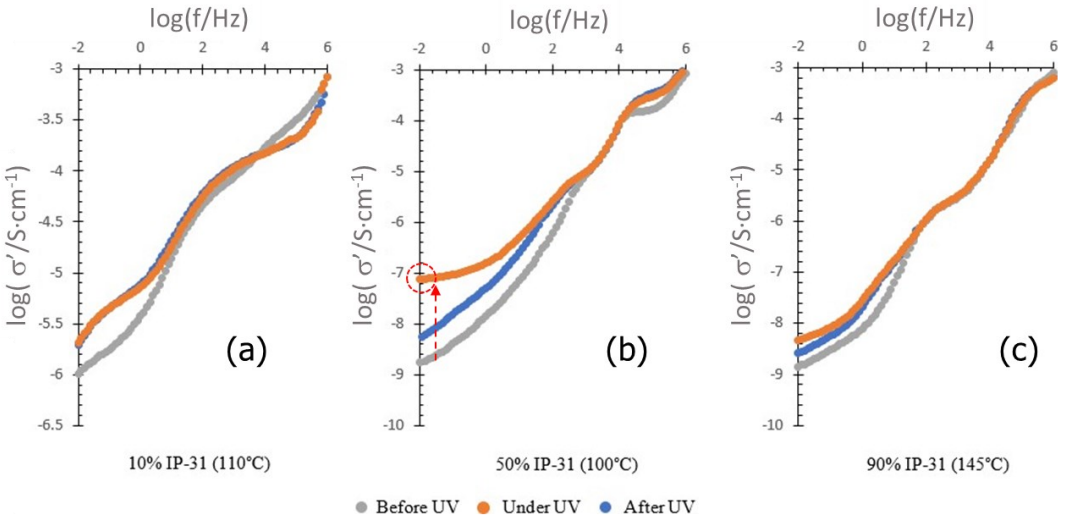

Figure 11. Frequency dependence of the real component, σ', of the complex conductivity, σ*, measured at the mesophases of the light-responsive mixtures before (blue), during (orange) and after (grey) UV illumination (200 mW·cm^{-2}; 365 nm): **(a)**: 10%-IP31; **(b)** 50%-IP31; **(c)** 90%-IP31.

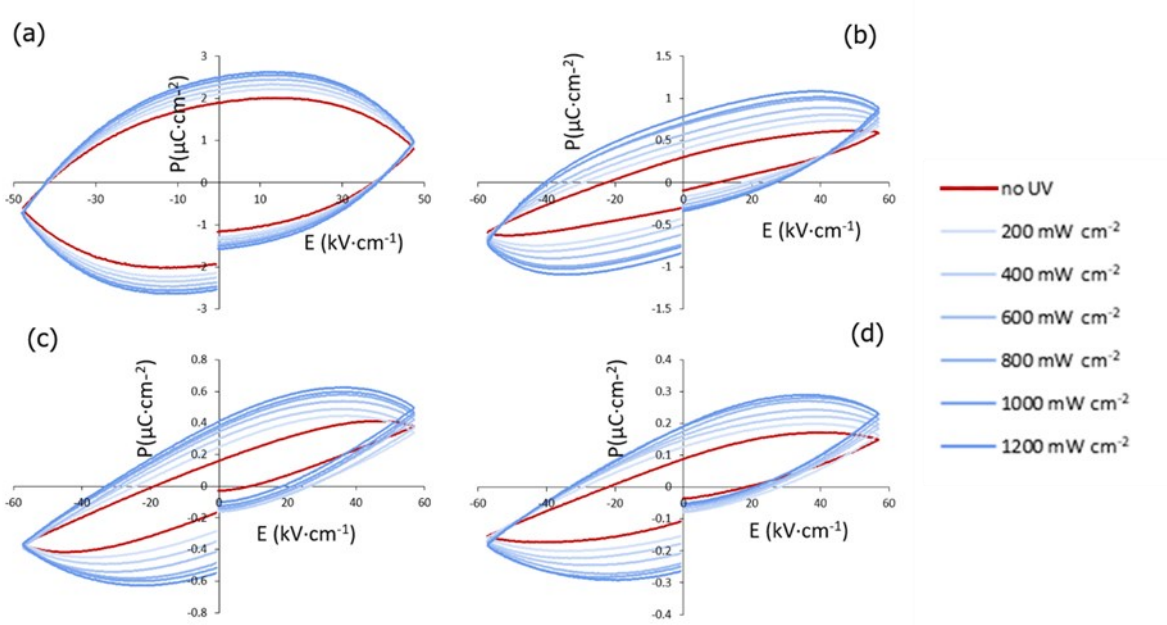

Figure 12. Hysteresis loops (polarisation, P, *vs* electrical field, E) showing the effect of UV-vis light irradiation (365 nm, 200 mW·cm^{-2}) on the ferroelectric response of 10%-IP31 (**a**, T=110^{o}C) , 50%-IP31 (**b**, T=100^{o}C), and 90%-IP31 (**c**: T=145^{o}C; **d**, T=162^{o}C) in their mesophase ranges, at 20Hz.

3.4. Density Functional Theory calculations

With the aim to further investigate correlations between the molecular structure and the properties studied in the previous sections, we have conducted a quantum mechanical density functional theory (DFT) study using the methodology listed in the molecular modelling section (*vide supra*), on four different molecular models of NG75-COO and IP31-AzB, including different *E* and *Z* isomers to account for the effect of photoisimerisation on the molecular configurations. The models have shorter terminal chains (*n* = 4) to economise computing resources without impacting the electronic distributions of the bent-core skeleton. **Fig. 13** displays the molecular electrostatic potential (MEP) distribution and optimised geometries of the models for: *NG75-COO*, IP31-AzB with both azobenzene groups in *E* conformation (*IP31-AzB-E_all*), IP31-AzB with both azobenzene groups isomerised into *Z* (*IP31-AzB-Z_all*), and IP31-AzB with only one azobenzene group isomerised into *Z* (*IP31-AzB-Z_E*). We speculate that *IP31-AzB-Z_E* may be useful to model partial isomerisation, attenuated light irradiation dosage, or low IP31-AzB concentrations.

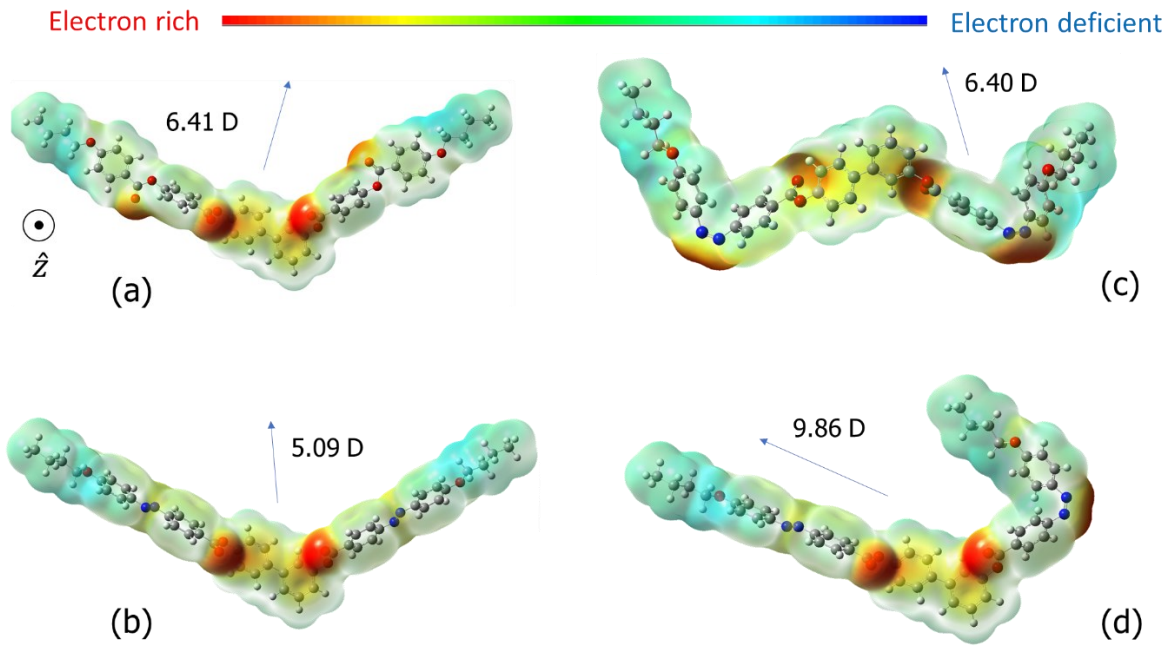

Figure 13. Molecular Electrostatic Potential (MEP) distributions estimated from the DFT calculations for the four model molecules under study: (**a**) *NG75*; (**b**) *IP31-trans_all*; (**c**) *IP31-cis_all*; (**d**) *IP31-cis_trans*. Arrows indicate direction of the estimated molecular dipole moment. Scale represents electron rich (red) *vs* electron deficient (blue) regions (arbitrary units).

Based on the molecular structure we expect that and was confirmed by molecular electrostatic potential (MEP) maps in **Fig. 13**, the distribution of probable electrophilic (red region) attack sites are around the central part of the molecules. Indeed, the substitution of two esters by azobenzene groups drops the molecular dipole moment of *IP31-AzB-E_all* by 1.5D, in comparison to *NG75-COO*. This is consistent with the lower dielectric response of the IP31-AzB richer mixtures observed in section 3.2. Despite their evident similarities, there are two interesting observations we can make based on the optimised geometries of *NG75-COO* and *IP31-AzB-E_all* in **Fig. 13(a)** and **(b)**, respectively. First, *NG75-COO* displays four aromatic rings in the same $\hat{z}$ plane, almost perpendicular to the strong C=O dipoles, whilst in *IP31-AzB-E_all*, the azobenzene groups in opposite branches and the central biphenyl group are in different planes. Second, two neighbouring NG75-COO molecules (stuck

through the $\hat{z}$ plane) could benefit from complementary dipole-dipole and π-π stacking interactions in various parts of the molecule. These interactions and packing arrangement seem more limited in *IP31-AzB-E_all*, and that could explain why the compound tends to form columnar phases, and cannot sustain smectic periodicity through several molecular aggregates. Hence, the drop in mesophase stability for NG75-COO-rich mixtures in the phase diagram, **Fig. 4**, cannot be justified solely in terms of molecular geometry or packing, and the different local interactions may play an important role in the phase behaviour of the NG75-COO/IP31-AzB system.

The *E*-to-*Z* isomerisation of the azobenzene group results in a new local dipole moment located at the N=N bond, and as a result, *IP31-AzB-Z_all* and *IP31-AzB-Z_E* have larger dipole moments than *IP31-AzB-E_all*. This is consistent with the increase in the dielectric and ferroelectric responses on illumination, see again **Fig. 11** and **12**. Indeed, the *IP31-AzB-Z_E* model shows the highest dipole moment of the series, close to 10D, due to the lack of cancellation of the second azobenzene group, and suggests that relatively low concentrations of azobenzene groups can have a huge impact on the polar properties and responses of the compounds. The geometry of the *Z* isomers, **Fig. 13(c)** and **(d)**, deviates from the V-shape of the original bent-cores, **Fig. 13(a)** and **(b)**, which again justifies that photoisomerisation can promote breakage of the liquid crystal order and further isotropisation, see again **Fig. 9(c)**. Interestingly, the optimised geometry of *IP31-AzB-Z_E* has some similarities to hockey-stick molecules with crossover structures between BCLCs and linear rod-like(calamitic) molecules. Our results suggest that such geometries, which include some component of further symmetry breaking, could be induced and modulated by the application of external stimuli, such as, light irradiation, leading to improved physical response (i.e., electrical response).

We have also calculated the energy difference between the highest occupied and lowest unoccupied molecular orbitals HOMO/LUMO for the ground, cationic (+1), anionic (-1), and excited states (multiplicity = 3) of the four models. Interestingly, the energy gap is considerably lower for *IP31-all_trans* (-1.92 eV) than for *NG75* (-2.59 eV), with the minimum

reached for *IP31-trans_cis* (-1.72 eV), see **Fig. S6**. This can reflect on the possibility of exciting azobenzene compounds facilitated by *trans*-to-*cis* photoisomerization. In ionised and excited states, **Fig. S7** to **S10**, more symmetrical and distributed charges are found compared to the ground state, even at HOMO levels, and the split in orbitals also lead to small energy differences (see **Tables S2** and **S3**). These results could be relevant to explain the dielectric and ferroelectric response of the bent-core materials to electric fields, and will be the focus of further investigations.

4. Conclusions

The NG75-COO/IP31-AzB binary mixtures, combining two bent-core liquid crystal compounds, one of them with azobenzene units, show good compatibility and mesomorphism in the whole composition range, with some reductions in the clearing points and liquid crystalline ranges. The majority component controls the mesomorphism, resulting in smectic and columnar phases. Whilst NG75-COO, SmCP inducer, promotes strong dielectric, ferroelectric and conductivity response to the mixtures, the introduction of IP31-AzB confers them photoresponsive character *via E*-to-*Z* photoisomerisation of their azobenzene group. Photoisomerisation upon UV irradiation enhances the dielectric and ferroelectric response of the mixtures while retaining the liquid crystalline order under mild irradiation conditions, *via* an increase in the molecular dipole moment assessed by DFT, and with a reduction of the energy barrier between HOMO and LUMO states.

Our compositional analysis highlights that the equimolar mixture, 50%-IP31-AzB, displays a balanced combination of responsive properties, which allows for reversible switching of conductivity (with two orders of magnitudes increase upon irradiation) and cyclic performance, albeit its smectic range is depressed respect to the pristine components. Our findings suggest that smectic bent-core phases are more adequate to develop responsive materials for energy conversion devices, and mechanisms to increase the ferroelectricity and conductivity will be further investigated, including the introduction of light-responsive dopants that can disrupt the liquid crystalline order.

Acknowledgements

IDC would like to thank the Universitat Politècnica de València (UPV), for the FPI grant (PAID-2019-SP20190013), the Generalitat Valenciana (GVA) and the European Social Fund (ESF), for the FPI grant (ACIF/2020/233) and the mobility grant (CIBEFP/2022/45). AMF would like to thank the Carnegie Trust for the Universities of Scotland, for the Research Incentive Grant RIG008586, the Royal Society and Specac Ltd., for the Research Grant RGS\R1\201397, the Royal Society of Chemistry for the award of a mobility grant (M19-0000), the Scottish Government and the Royal Society of Edinburgh for the award of a SAPHIRE project, NHS Scotland for the 20/016 R&D Endowments Award, and the University of Aberdeen for the CF10801-10 and CF10723-44 pump priming grants. The authors from INMA greatly appreciate financial support from projects of the Spanish Government

PID2021-122882NB-I00 [MCIU/AEI/FEDER, UE] and the Gobierno de Aragón/FEDER (research group E47_23R); and C.A-S for the FPI Fellowship PRE2019-090773. Thanks are given to the nuclear magnetic resonance, mass spectrometry, and thermal analysis services of CEQMA (Univ. Zaragoza-CSIC). BC is grateful to the National Science Foundation for supporting this work under grant no. CHE- 2306317. BC also thanks Illinois State University (ISU) for their financial support through university research grant (URG). Computational work is performed using resources from High Performance Computing (HPC) at Illinois State University.

Data availability statement

The raw/processed data required to reproduce these findings cannot be shared at this time due to technical or time limitations.

References

1. Martinez-Felipe, A., *Liquid crystal polymers and ionomers for membrane applications.* Liquid Crystals, 2011. **38**(11-12): p. 1607-1626.
2. Kato, T., et al., *Functional Liquid Crystals towards the Next Generation of Materials.* Angewandte Chemie-International Edition, 2018. **57**(16): p. 4355-4371.
3. Uchida, J., et al., *Advanced Functional Liquid Crystals.* Advanced Materials, 2022. **34**(23).
4. Yoshio, M., et al., *One-dimensional ion-conductive polymer films: Alignment and fixation of ionic channels formed by self-organization of polymerizable columnar liquid crystals.* Journal of the American Chemical Society, 2006. **128**(16): p. 5570-5577.
5. Kishimoto, K., et al., *Nano-segregated polymeric film exhibiting high ionic conductivities* Journal of the American Chemical Society, 2005. **127**(44): p. 15618-15623.
6. Zhang, H., et al., *From Channel-Forming Ionic Liquid Crystals Exhibiting Humidity-Induced Phase Transitions to Nanostructured Ion-Conducting Polymer Membranes.* Advanced Materials, 2013. **25**(26): p. 3543-3548.
7. Ichikawa, T., *Zwitterions as building blocks for functional liquid crystals and block copolymers.* Polymer Journal, 2017. **49**(5): p. 413-421.
8. Ichikawa, T., T. Kato, and H. Ohno, *3D Continuous Water Nanosheet as a Gyroid Minimal Surface Formed by Bicontinuous Cubic Liquid-Crystalline Zwitterions.* Journal of the American Chemical Society, 2012. **134**(28): p. 11354-11357.
9. Ueda, S., et al., *Anisotropic Proton-Conductive Materials Formed by the Self-Organization of Phosphonium-Type Zwitterions.* Advanced Materials, 2011. **23**(27): p. 3071-+.
10. Concellon, A., et al., *Proton conductive ionic liquid crystalline poly(ethyleneimine) polymers functionalized with oxadiazole.* Rsc Advances, 2018. **8**(66): p. 37700-37706.
11. Concellon, A., et al., *Proton-conductive materials formed by coumarin photocrosslinked ionic liquid crystal dendrimers.* Journal of Materials Chemistry C, 2018. **6**(5): p. 1000-1007.
12. Alauddin, S.M., et al., *New side-chain liquid crystalline terpolymers with anhydrous conductivity: Effect of azobenzene substitution on light response and charge transfer.* European Polymer Journal, 2021. **146**: p. 110246-110246.
13. Alauddin, S.M., et al., *Liquid Crystalline Copolymers Containing Sulfonic and Light-Responsive Groups: From Molecular Design to Conductivity.* Molecules, 2020. **25**(11).
14. Vanti, L., et al., *Ionically conducting and photoresponsive liquid crystalline terpolymers: Towards multifunctional polymer electrolytes*. 2018. p. 124-132.
15. Hogberg, D., et al., *Self-Assembled Liquid-Crystalline Ion Conductors in Dye-Sensitized Solar Cells: Effects of Molecular Sensitizers on Their Performance.* Chempluschem, 2017. **82**(6): p. 834-840.
16. Hogberg, D., et al., *Liquid-Crystalline Dye-Sensitized Solar Cells: Design of Two-Dimensional Molecular Assemblies for Efficient Ion Transport and Thermal Stability.* Chemistry of Materials, 2016. **28**(18): p. 6493-6500.
17. Kumar, M. and S. Kumar, *Liquid crystals in photovoltaics: a new generation of organic photovoltaics.* Polymer Journal, 2017. **49**(1): p. 85-111.

18. Wang, S., et al., *An ionic liquid crystal-based solid polymer electrolyte with desirable ion-conducting channels for superior performance ambient-temperature lithium batteries.* Polymer Chemistry, 2018. **9**(37): p. 4674-4682.

19. Wang, S., et al., *High-Performance All-Solid-State Polymer Electrolyte with Controllable Conductivity Pathway Formed by Self-Assembly of Reactive Discogen and Immobilized via a Facile Photopolymerization for a Lithium-Ion Battery.* Acs Applied Materials & Interfaces, 2018. **10**(30): p. 25273-25284.

20. Kuwabara, A., et al., *Nanostructured liquid-crystalline Li-ion conductors with high oxidation resistance: molecular design strategy towards safe and high-voltage-operation Li-ion batteries.* Chemical Science, 2020. **11**(39): p. 10631-10637.

21. Sakuda, J., et al., *Liquid-Crystalline Electrolytes for Lithium-Ion Batteries: Ordered Assemblies of a Mesogen-Containing Carbonate and a Lithium Salt.* Advanced Functional Materials, 2015. **25**(8): p. 1206-1212.

22. Lee, M.H. and W.Z. Wu, *2D Materials for Wearable Energy Harvesting.* Advanced Materials Technologies, 2022. **7**(9).

23. Kato, T., et al., *Transport of ions and electrons in nanostructured liquid crystals.* Nature Reviews Materials, 2017. **2**(4).

24. Ju, Z.Y., et al., *Vertically aligned two-dimensional materials-based thick electrodes for scalable energy storage systems.* Nano Research, 2021. **14**(10): p. 3562-3575.

25. Jiang, X.N., W.B. Huang, and S.J. Zhang, *Flexoelectric nano-generator: Materials, structures and devices.* Nano Energy, 2013. **2**(6): p. 1079-1092.

26. Dominguez-Candela, I., et al., *Light-responsive bent-core liquid crystals as candidates for energy conversion and storage.* Journal of Materials Chemistry C, 2022. **10**(48): p. 18200-18212.

27. Martinez-Felipe, A., et al., *Bent-core liquid crystals joining the ethylene-oxide/lithium ion tandem: Ionic conductivity and dielectric response towards new electrolytes for energy applications.* Journal of Molecular Liquids, 2023. **390**: p. 123100.

28. Etxebarria, J. and M.B. Ros, *Bent-core liquid crystals in the route to functional materials.* Journal of Materials Chemistry, 2008. **18**(25): p. 2919-2926.

29. Reddy, R.A. and C. Tschierske, *Bent-core liquid crystals: polar order, superstructural chirality and spontaneous desymmetrisation in soft matter systems.* Journal of Materials Chemistry, 2006. **16**(10): p. 907-961.

30. Takezoe, H. and Y. Takanishi, *Bent-core liquid crystals: Their mysterious and attractive world.* Japanese Journal of Applied Physics Part 1-Regular Papers Brief Communications & Review Papers, 2006. **45**(2A): p. 597-625.

31. Tschierske, C., *Development of Structural Complexity by Liquid-Crystal Self-assembly.* Angewandte Chemie-International Edition, 2013. **52**(34): p. 8828-8878.

32. Eremin, A. and A. Jakli, *Polar bent-shape liquid crystals - from molecular bend to layer splay and chirality.* Soft Matter, 2013. **9**(3): p. 615-637.

33. Kato, T. and Y. Kamikawa, *Hydrogen-Bonded Systems: Discrete Defined Aggregates by Intermolecular H-Bonding, Amides, Carboxylic Acids, and Heterocycles,* , in *Handbook of Liquid Crystals, 8 Volume Set, 2nd Edition*, J.W. Goodby, et al., Editors. 2014, Wiley. p. 513-540.

34. Takezoe, H. and A. Eremin, *Bent-Shaped Liquid Crystals: Structures and Physical Properties*, in *Bent-Shaped Liquid Crystals: Structures and Physical Properties*. 2017.

35. Takezoe, H., *Polar liquid crystals - ferro, antiferro, banana, and columnar.* Molecular Crystals and Liquid Crystals, 2017. **646**(1): p. 46-65.

36. Le, K.V., H. Takezoe, and F. Araoka, *Chiral Superstructure Mesophases of Achiral Bent-Shaped Molecules - Hierarchical Chirality Amplification and Physical Properties.* Advanced Materials, 2017. **29**(25).

37. Niori, T., et al., *Distinct ferroelectric smectic liquid crystals consisting of banana shaped achiral molecules.* Journal of Materials Chemistry, 1996. **6**(7): p. 1231-1233.

38. Niigawa, Y., et al., *Polar structures in binary mixtures of bent-core liquid crystals showing ferroelectric and antiferroelectric B2 phases.* Physical Review E, 2007. **76**(3).

39. Anjali, S. and R. Pratibha, *Synchronization of conformational chirality in mixtures of achiral bent-core molecules.* Rsc Advances, 2016. **6**(59): p. 53830-53838.

40. Liu, J., et al., *Binary mixtures of bent-core molecules forming distinct types of B4 phase nano- and microfilament morphologies.* Liquid Crystals, 2021. **48**(8): p. 1129-1139.

41. Wang, J.R., et al., *Wide temperature-range, multi-component, optically isotropic antiferroelectric bent-core liquid crystal mixtures for display applications.* Liquid Crystals, 2018. **45**(3): p. 333-340.

42. Jain, V., et al., *Imine-based highly polar achiral unsymmetrical four-ring bent shaped liquid crystals: Design, synthesis and characterization.* Journal of Molecular Structure, 2022. **1267**.

43. Bobrovsky, A.Y., et al., *Photoinduced Split of the Cavity Mode in Photonic Crystals Based on Porous Silicon Filled with Photochromic Azobenzene-Containing Substances.* Acs Applied Polymer Materials, 2022. **4**(10): p. 7387-7396.

44. Bobrovsky, A., et al., *Photo-optical properties of amorphous and crystalline films of azobenzene-containing photochromes with bent-shaped molecular structure.* Journal of Photochemistry and Photobiology a-Chemistry, 2016. **316**: p. 75-87.

45. Folcia, C.L., et al., *Achiral bent-core liquid crystals with azo and azoxy linkages: Structural and nonlinear optical properties and photoisomerization.* Chemistry of Materials, 2006. **18**(19): p. 4617-4626.

46. Ortega, J., et al., *Electric-field-induced phase transitions in bent-core mesogens determined by x-ray diffraction.* Physical Review E, 2011. **84**(2).

47. Shen, D., et al., *Molecular Design of Nonchiral Bent-Core Liquid Crystals with Antiferroelectric Properties.* Journal of the American Chemical Society, 2000. **122**(8): p. 1593-1601.

48. Gimeno, N., et al., *Terminal Chains as a Tool To Modulate the Properties of Bent-Core Liquid Crystals.* Chemistry of Materials, 2009. **21**(19): p. 4620-4630.

49. Pintre, I.C., et al., *Liquid crystalline and nonlinear optical properties of bent-shaped compounds derived from 3,4'-biphenylene.* Journal of Materials Chemistry, 2007. **17**(21): p. 2219-2227.

50. Frisch, M.J., et al., *Gaussian (Revision D. 01) Gaussian Inc, Wallingford, CT*. 2009: US.

51. Grimme, S., *Semiempirical GGA-type density functional constructed with a long-range dispersion correction.* Journal of Computational Chemistry, 2006. **27**(15): p. 1787-1799.

52. Ovalle, S. and C. Malardier-Jugroot, *Choice of functional for iron porphyrin density functional theory studies: Geometry, spin-state, and binding energy analysis.* Computational and Theoretical Chemistry, 2022. **1213**.

53. Minenkov, Y., et al., *The accuracy of DFT-optimized geometries of functional transition metal compounds: a validation study of catalysts for olefin metathesis and other reactions in the homogeneous phase.* Dalton Transactions, 2012. **41**(18): p. 5526-5541.

54. Eriksson, E.S.E. and L.A. Eriksson, *Predictive power of long-range corrected functionals on the spectroscopic properties of tetrapyrrole derivatives for photodynamic therapy.* Physical Chemistry Chemical Physics, 2011. **13**(15): p. 7207-7217.

55. Rassolov, V.A., et al., *6-31G* basis set for atoms K through Zn.* Journal of Chemical Physics, 1998. **109**(4): p. 1223-1229.

56. Guo, L.F., et al., *Ferroelectric behavior of orthogonal smectic phase made of bent-core molecules.* Physical Review E, 2011. **84**(3).

57. Guo, L., et al., *Transition between two orthogonal polar phases in symmetric bent-core liquid crystals.* Soft Matter, 2011. **7**(6): p. 2895-2899.

58. Dunmur, D.A., et al., *Dielectric studies of liquid crystals: the influence of molecular shape.* Liquid Crystals, 2010. **37**(6-7): p. 723-736.

59. Martinez-Felipe, A., et al., *Characterization of Functionalized Side-Chain Liquid Crystal Methacrylates Containing Nonmesogenic Units by Dielectric Spectroscopy.* Industrial & Engineering Chemistry Research, 2013. **52**(26): p. 8722-8731.

60. Yildiz, A., et al., *The role of temperature on dielectric relaxation and conductivity mechanism of dark conglomerate liquid crystal phase.* Physica B-Condensed Matter, 2016. **485**: p. 21-28.

61. Bhowmik, P.K., *Dicationic Ionic Liquids based on Bis(4-oligoethyleneoxyphenyl) Viologen Bistriflimide Salts Exhibiting High Ionic Conductivities.* Journal of Molecular Liquids, 2022.

62. Bhowmik, P.K., et al., *Dicationic stilbazolium salts: Structural, thermal, optical, and ionic conduction properties.* Journal of Molecular Liquids, 2021. **341**.

63. Bhowmik, P.K., et al., *Ionic liquid crystals: Synthesis and characterization via NMR, DSC, POM, X-ray diffraction and ionic conductivity of asymmetric viologen bistriflimide salts.* Journal of Molecular Liquids, 2021. **328**: p. 115370-115370.

64. Vallerien, S.U., et al., *Field-Dependent Soft and Goldstone Mode in a Ferroelectric Liquid-Crystal as Studied by Dielectric-Spectroscopy.* Physics Letters a, 1989. **138**(4-5): p. 219-222.

65. Gouda, F., K. Skarp, and S.T. Lagerwall, *Dielectric studies of the soft mode and Goldstone mode in ferroelectric liquid crystals.* Ferroelectrics, 1991. **113**(1): p. 165-206.

66. Kumar, G.S. and D.C. Neckers, *Photochemistry of Azobenzene-Containing Polymers.* Chemical reviews, 1989. **89**(8): p. 1915-1925.

67. Hegde, G., et al., *Synthesis and liquid crystalline behaviour of substituted (E)-phenyl-4-(phenyldiazenyl) benzoate derivatives and their photo switching ability.* Liquid Crystals, 2016. **43**(11): p. 1578-1588.

68. Sunil, B.N., et al., *Influence of inter- and intramolecular H-bonding on the mesomorphic and photoswitching behaviour of (E)-4-((4-(hexyloxy)phenyl)diazenyl)-N-phenyl benzamides.* Rsc Advances, 2020. **10**(34): p. 20222-20230.

69. Alaasar, M., *Azobenzene-containing bent-core liquid crystals: an overview.* Liquid Crystals, 2016. **43**(13-15): p. 2208-2243.

70. Sunil, B.N., et al., *Effective tuning of optical storage devices using photosensitive bent-core liquid crystals.* Journal of Molecular Liquids, 2020. **304**.

71. Velayutham, T.S., et al., *A new light-responsive resistive random-access memory device containing hydrogen-bonded complexes.* Journal of Photochemistry and Photobiology A: Chemistry, 2021. **404**: p. 112914.

72. Ranjitha, B.S., et al., *Impact of terminal group on azobenzene liquid crystal dimers for photo-responsive optical storage devices.* Journal of Molecular Liquids, 2023. **383**.

73. Zaton, D., et al., *Photo-driven effects in twist-bend nematic phases: Dynamic and memory response of liquid crystalline dimers.* Journal of Molecular Liquids, 2021. **344**: p. 117680.

74. Paterson, D.A., et al., *Reversible Isothermal Twist-Bend Nematic-Nematic Phase Transition Driven by the Photoisomerization of an Azobenzene-Based Nonsymmetric Liquid Crystal Dinner.* Journal of the American Chemical Society, 2016. **138**(16): p. 5283-5289.

75. Prasad, S.K., et al., *A soft-bent dimer composite exhibiting twist-bend nematic phase: Photo-driven effects and an optical memory device.* Applied Physics Letters, 2018. **112**(25).

76. Prasad, S.K., et al., *Photoinduced effects in nematic liquid crystals.* Phase Transitions, 2005. **78**(6): p. 443-455.

77. Ibrahim, A.R., et al., *p-Methoxy Azobenzene Terpolymer as a Promising Energy-Storage Liquid Crystal System.* Journal of Physical Chemistry C, 2021. **125**(41): p. 22472-22482.